

# The 2004 earthquakes offshore of the Kii peninsula, Japan: Hypocentral relocation, source process and tectonic implication

Ling Bai<sup>a,\*</sup>, Eric A. Bergman<sup>b</sup>, E. Robert Engdahl<sup>b</sup>, Ichiro Kawasaki<sup>a</sup>

<sup>a</sup> Disaster Prevention Research Institute, Kyoto University, Gokasho, Uji 611-0011, Japan

<sup>b</sup> Department of Physics, University of Colorado, Boulder, CO 80309-0390, USA

Received 23 August 2006; received in revised form 28 May 2007; accepted 24 July 2007

## Abstract

On 5 September 2004, two major earthquakes of  $M_W$  7.2 and  $M_W$  7.3 (referred to as the foreshock and the mainshock hereafter) occurred close to the Nankai Trough in southwest Japan. This earthquake sequence is located within the subducting Philippine Sea plate (PHS) with an aftershock distribution that overlapped a portion of the source region of the 1944 Tonankai earthquake ( $M_W$  7.9). We relocate 53 events with magnitudes greater than 4.2 by combining a single-event location method for depth and a multiple-event location method for epicenter and origin time. Source mechanisms and rupture histories of the foreshock and the mainshock are investigated by using a waveform modeling method, which allows for mechanism changes during the rupture process. The  $M_W$  7.2 foreshock and the  $M_W$  7.3 mainshock are relocated in the uppermost mantle of the PHS on primary high-angle reverse faults. Focal mechanisms are consistent with the horizontal and vertical projects of the distribution of aftershocks. We speculate that this earthquake sequence was due to the collision reaction between the PHS and the Zenisu Ridge.

© 2007 Published by Elsevier B.V.

**Keywords:** Hypocentral location; Source process; Outer rise; Zenisu Ridge

## 1. Introduction

The Nankai Trough off densely populated southwestern Japan is one of the great-earthquake generating regions on the Earth, where the PHS is subducting beneath the overriding Eurasia plate at a convergence rate of around 4–6 cm/year (Seno et al., 1993). Historical documents since the seventh century showed that the recurrence interval of great magnitude eight class earthquakes was 100–150 years. The last great earthquakes occurred in 1944 and 1946, and the probability of the occurrence

for the next ones in the following 30 years is about 50% (the Headquarter of Earthquake Research Promotion, 2001). The 2004 earthquakes offshore of the Kii peninsula occurred close to the deformation front of the central Nankai Trough (Fig. 1). The aftershock distribution overlaps a portion of the source region of the 1944 Tonankai earthquake ( $M_W$  7.9) (Kikuchi et al., 2003). In this study, we investigate spatial and temporal variations in seismicity and source process of the 2004 earthquake sequence.

Locating earthquakes in offshore regions is problematic. Since seismological stations are mostly located in onshore areas, the insufficient azimuthal coverage of regional stations leads to uncertainties in the focal depth determination by several tens of kilometers (Richards et al., 2006). Ocean Bottom Seismographs (OBS) were deployed to help constrain the locations of after shocks (Sakai et al., 2005). Most of the hypocenters located by

\* Corresponding author. Present address: Earthquake Research Institute, University of Tokyo, 1-1-1 Yayoi, Bunkyo-ku, Tokyo 113-0032, Japan.

E-mail address: [bai@eri.u-tokyo.ac.jp](mailto:bai@eri.u-tokyo.ac.jp) (L. Bai).

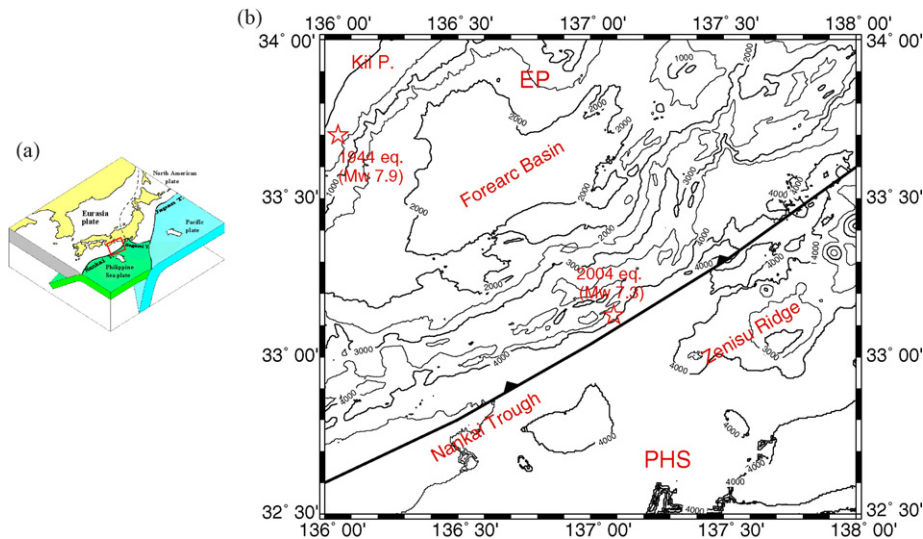


Fig. 1. (a) Location (the red rectangle) and (b) interpretation of the study area. The PHS is subducting beneath the overriding Eurasia Plate at a convergence rate of around 4–6 cm/year. The region is divided into three tectonic units: Forearc Basin, Nankai Trough, and Zenisu Ridge (Wu et al., 2005). The initial rupture points of the 1944 Tonankai earthquake (Kanamori, 1972) and the 2004 earthquake offshore of the Kii peninsula (relocated in this study) are also shown. The isobaths are at a depth interval of 500 m. Numbers on them indicate the depth in meters. (For interpretation of the references to color in this figure legend, the reader is referred to the web version of the article).

OBS data were shallower than 30 km, whereas most of the hypocenters by the Japan Meteorological Agency (JMA) using onshore observations were deeper than 30 km. However, earthquakes with magnitudes greater than 4.0 or so cannot be located accurately using OBS data because of the limited dynamic range of the OBS recording system (Sakai et al., 2005).

In this study, we focus our efforts toward better locations of 53 events with magnitudes greater than 4.2 using regional and teleseismic data. We first relocate earthquakes based on a single-event location method with special attention to the correct association of depth phases. Using the single-event locations as starting values, we improve the accuracy of relative locations using a multiple-event location method. We also employ a teleseismic waveform inversion method to constrain source mechanisms and rupture histories of the foreshock and the mainshock. Particular attention was paid to the trade-off between focal depth and variance of waveform modeling. Based on the accurate source parameters we further discuss the tectonic implications.

## 2. Hypocentral relocation from regional and teleseismic data

### 2.1. Method and data

The EHB (abbreviated from the initial letters of three authors: Engdahl et al., 1998) is a single-event location

method. The elements of the algorithm that contribute to the improvements of location accuracy include: (1) use of the arrival times of PKiKP, PKPdf, and the teleseismic depth phases pP, pwP, and sP, in addition to regional and teleseismic P and S phases; (2) iterative relocation with dynamic phase identification; (3) use of an improved 1D global travel time model, ak135 (with a water layer) (Kennett et al., 1995); (4) ellipticity corrections for the ak135 model; (5) empirical teleseismic station patch corrections (for  $5^\circ \times 5^\circ$  patches); (6) weighting by phase variance as a function of distance; and (7) selection criteria for events having 10 or more observations at teleseismic distances ( $>28^\circ$ ) and a teleseismic secondary azimuth gap  $<180^\circ$  (Engdahl, 2006; Engdahl et al., 2006).

Starting from the EHB locations, we further improve the accuracy of relative location using the Hypocentroidal Decomposition (HDC) method (Jordan and Sverdrup, 1981; newly developed by E.A. Bergman). The hypocentroid of an event cluster is defined to be the average location of events within the cluster, and individual epicenters are determined based on the deviations from the hypocentroid. Depths are held fixed at the values determined in the EHB processing. This method has been used extensively in many studies (Ritzwoller et al., 2003; Bondár et al., 2004; Rastogi et al., 2005) and is well suited for this study for several reasons. The HDC is a highly developed tool for relative earthquake location at regional and teleseismic distances. It uses

all available information in the data set, no data are discarded for making the problem more tractable. For a large data sets, the HDC is computationally efficient, requiring the solution of smaller matrices than some other methods. At each iteration, the hypocentroid and cluster vectors (i.e., both absolute and relative locations) are updated.

One of the advantages of multiple event relocation is the ability to use repeated observations to estimate the empirical reading error for each specific station-phase. We use a robust estimation method for this purpose, so that outliers do not bias the estimate. In turn, the empirical reading errors allow us to more accurately identify outliers in the arrival time dataset. Outliers are flagged to achieve a pseudo-normal distribution for each station-phase combination. Proper estimation of reading errors and elimination of outliers helps ensure the reliability of confidence ellipses for relative locations.

The U.S. Geological Survey's Earthquake Data Report catalog contained 53 events in the source region

with magnitudes greater than 4.2 from 5 September 2004 to 30 April 2005. In the EHB processing, we use arrival times for first-arriving P and S phases (excluding distances greater than  $100^\circ$  for P and  $80^\circ$  for S), PKiKP (at distances greater than  $110^\circ$ ), PKPdf (excluding distances near the PKP caustic), and the depth phases pP, pwP, and sP (excluding distances less than  $30^\circ$ ). We use 5562 arrival times from 857 stations at regional (distances greater than  $1^\circ$ ) and teleseismic distances to constrain the relative locations (cluster vectors). The hypocentroid of the cluster, which sets the absolute coordinates, is estimated with 3766 P arrivals from 602 stations, at epicentral distances from  $30^\circ$  to  $100^\circ$  (Fig. 2). All these stations represent a good azimuthal coverage around the earthquake cluster. Theoretical travel times are calculated from the ak135 Earth model, which provides a better fit to the global travel-time data than that from the iasp91 (Kennett and Engdahl, 1991) and the Jefferey–Bullen (Jeffreys and Bullen, 1940) travel-time tables.

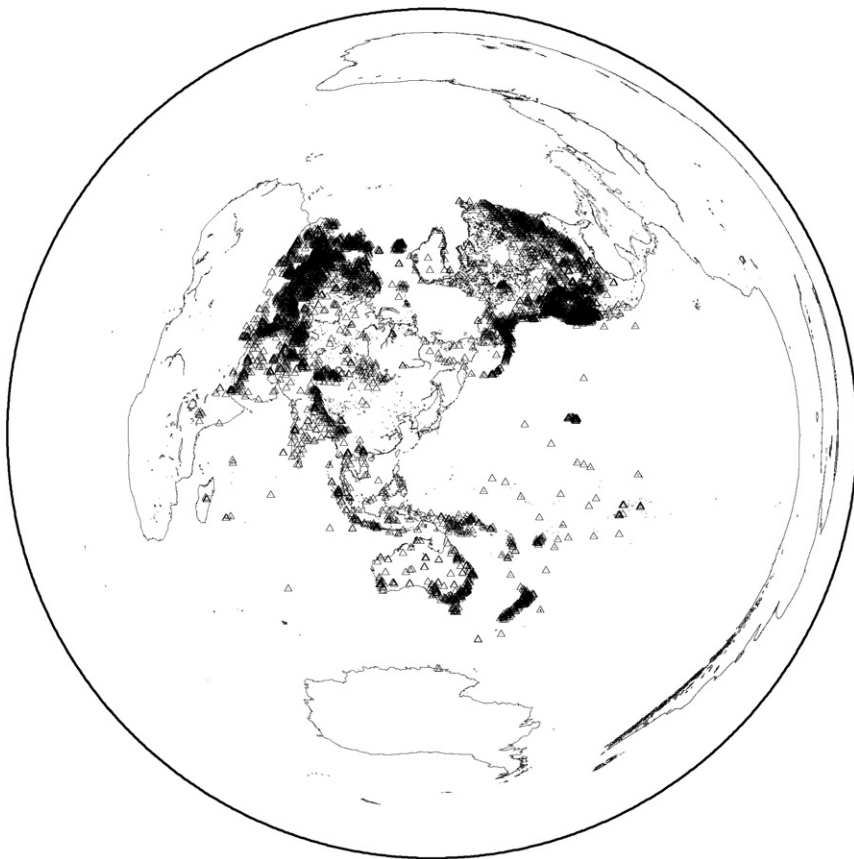


Fig. 2. Stations (open triangles) with epicentral distances from  $30^\circ$  to  $100^\circ$  used in HDC method. The location of the earthquake cluster is at the center of this figure.

Table 1

Hypocenters of 53 earthquakes relocated by using the combined EHB method for depth and HDC method for epicenter and origin time

Nos.	Date	Time	$\varphi_N$ (°)	$\lambda_E$ (°)	$H$ (km)	$M_W$	N1	N2	Area (km <sup>2</sup> )
1	2004.09.05	10:07:07.27	33.013	136.658	18.3	7.2	896	30	3
2	2004.09.05	10:17:34.16	32.940	136.819	15.0	5.1	54	0	28
3	2004.09.05	10:25:42.22	33.043	136.659	15.0	4.7	60	1	18
4	2004.09.05	11:15:59.12	33.067	137.103	17.5	4.5	34	7	40
5	2005.09.05	12:01:14.71	32.915	136.849	25.0	4.3	35	9	52
6	2004.09.05	12:36:19.45	32.938	136.855	23.9	4.3	43	10	36
7	2004.09.05	12:42:20.53	32.998	136.830	25.0	4.5	33	5	60
8	2004.09.05	14:57:21.18	33.132	137.087	17.6	7.3	997	137	4
9	2004.09.05	15:26:59.54	33.256	137.022	17.5	4.8	99	27	11
10	2004.09.05	15:53:19.80	33.181	137.115	16.0	4.7	99	12	23
11	2004.09.05	15:59:24.54	33.036	137.127	23.5	4.4	35	10	66
12	2004.09.05	16:06:43.79	33.211	136.804	16.3	4.5	59	14	18
13	2004.09.05	16:12:25.54	33.019	136.900	15.0	4.5	41	11	35
14	2004.09.05	16:13:57.14	32.993	136.897	25.8	4.5	42	8	45
15	2004.09.05	16:15:00.71	33.149	137.122	18.0	4.8	68	10	18
16	2004.09.05	16:16:38.45	33.051	137.248	16.7	4.6	43	6	41
17	2004.09.05	16:53:20.21	33.266	136.847	15.0	4.4	32	2	45
18	2004.09.05	17:19:35.04	33.315	136.934	15.0	4.6	64	0	26
19	2004.09.05	17:34:10.66	32.984	136.823	15.2	4.6	81	20	21
20	2004.09.05	18:13:46.14	33.327	137.026	15.0	4.8	97	1	10
21	2004.09.05	20:31:00.87	33.266	136.786	17.4	5.2	287	25	11
22	2004.09.05	22:48:45.43	33.114	137.086	25.3	4.7	104	10	10
23	2004.09.05	24:20:50.70	33.241	136.818	16.0	4.5	61	14	34
24	2004.09.05	24:59:39.37	33.471	136.753	18.0	4.4	40	6	35
25	2004.09.06	00:01:44.88	33.035	136.920	26.5	4.3	50	6	35
26	2004.09.06	06:35:46.99	33.251	136.759	12.6	4.6	32	7	90
27	2004.09.06	06:46:49.33	33.498	136.703	15.0	4.4	37	0	50
28	2004.09.06	06:54:35.71	33.499	136.732	15.0	4.5	40	0	50
29	2004.09.06	10:20:32.10	33.088	137.377	22.1	4.6	60	15	28
30	2004.09.06	11:11:58.38	32.948	136.837	17.2	5.0	226	52	7
31	2004.09.06	12:39:48.40	33.100	137.118	15.9	4.5	34	5	27
32	2004.09.06	23:29:35.45	33.159	137.229	16.6	6.7	867	76	3
33	2004.09.07	03:10:36.43	33.257	136.820	15.0	4.6	22	0	21
34	2004.09.07	06:10:03.96	33.114	137.206	17.9	5.3	339	91	6
35	2004.09.07	18:36:22.64	33.204	137.112	25.0	5.4	445	14	3
36	2004.09.08	14:40:08.86	32.939	137.253	13.4	5.3	249	10	7
37	2004.09.08	14:58:25.03	33.131	137.190	10.8	6.7	752	41	5
38	2004.09.08	15:13:46.22	33.194	136.951	12.2	4.5	38	5	60
39	2004.09.08	16:03:55.00	33.096	136.896	15.0	4.3	32	0	51
40	2004.09.10	02:05:58.43	33.023	136.597	15.0	5.3	281	3	14
41	2004.09.16	18:56:28.97	32.842	136.588	13.6	4.4	51	9	52
42	2004.09.23	13:23:18.81	33.004	136.981	15.0	4.3	31	1	51
43	2004.09.30	21:40:13.13	33.020	137.080	15.0	4.4	32	0	35
44	2004.10.02	23:00:22.23	33.403	136.704	15.0	4.6	61	0	23
45	2004.10.10	10:54:00.95	32.981	136.874	15.0	4.4	28	0	52
46	2004.10.16	22:05:41.97	33.122	137.252	19.4	4.4	54	9	38
47	2004.11.18	20:46:25.80	33.118	137.192	15.0	4.7	72	2	24
48	2005.02.28	21:59:46.73	33.375	136.759	18.3	4.4	54	4	48
49	2005.03.14	10:49:30.75	33.083	136.992	15.0	4.5	59	1	15
50	2005.03.19	02:34:10.55	33.016	137.166	20.0	4.3	37	6	23
51	2005.04.08	11:33:24.31	33.031	136.922	15.0	4.2	31	0	29
52	2005.04.14	08:02:36.02	33.039	137.092	24.5	4.5	58	13	24
53	2005.04.22	08:54:17.28	33.084	136.904	15.0	4.6	32	0	26

Nos. is the number of event in origin time order. N1 and N2 are the numbers of all phase readings and depth phase readings, respectively. Area is the area in km<sup>2</sup> of the 90% confidence ellipse for relative location. The date and origin time are GMT time.

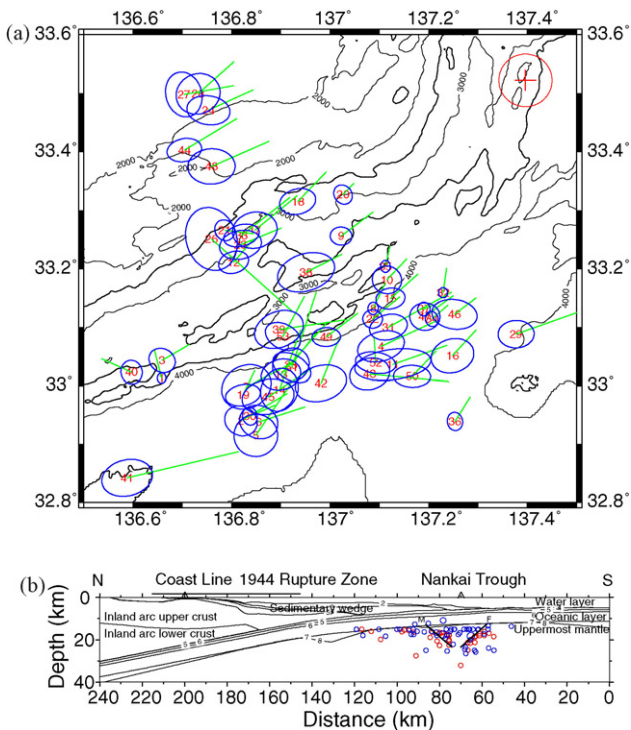


Fig. 3. (a) Map view of epicenters. The line from the center of each ellipse indicates the change in relative location from the starting location (EHB single-event location). Ellipses represent the 90% confidence limits on the relative locations. The circle at top right of the figure indicates a scale with 5 km radius. Event numbers are the same as in Table 1. The isobaths are the same as in Fig. 1(b). (b) Cross-section of relocated hypocenters along the N–S direction with 2D velocity boundaries. The blue circles show the hypocenters of the 53 events relocated in this study, while the red circles show the hypocenters of relatively smaller events relocated in a previous study (Bai et al., 2006). F and M are two major clusters across the foreshock and the mainshock (two large blue circles), respectively. The range with bold line on the upper of the figure indicates the surface projection of the rupture area of the 1944 Tonankai earthquake (Kikuchi et al., 2003). (For interpretation of the references to color in this figure legend, the reader is referred to the web version of the article).

## 2.2. Results of accurate relocation

The relocation results of the 53 events studied are listed in Table 1 with events numbers in origin time order. Fig. 3(a) shows a map view of their epicenters. The line connected to the center of each ellipse indicates the change in relative location from the starting EHB location. Ellipses are the 90% confidence limits on the relative location. The foreshock (No. 1) is located to the west, isolated from most of the other events. The mainshock (No. 8) and two strong aftershocks (Nos. 32 and 37) are located to the east, about 40 km from the foreshock. These four events are relocated with more than 750 phase readings, and consequently have very small

confidence ellipses. Event 26 is located with 32 phase readings and, although the quality of the location itself is not as high as most of the events in the cluster, it is co-located with many other events included in the cluster. Event 41 is as much as 30 km southwest from the foreshock. It is located with 51 phase readings and is judged to be susceptible to bias from a few outlier readings that may dominant the solution. For most events in the cluster, the uncertainty in relative epicentral location is in the range of 2–5 km at the 90% confidence level. On average the events are located about 5 km west-southwest from the initial single-event locations, but the relative locations are changed in complicated ways by the HDC analysis.

Fig. 3(b) shows a cross-section of relocated hypocenters along the N–S direction with 2D velocity boundaries (Nakanishi et al., 2002). The blue circles show the hypocenters of the 53 events relocated in this study, while the red circles show the hypocenters of relatively smaller events relocated in a previous study (Bai et al., 2006). The focal depth of all these events range between 10 and 33 km, shallower by about 20 km than those by JMA. Most events, including the foreshock and the mainshock are likely to be relocated in the uppermost mantle of the PHS. The relocated hypocenters show sharp images of seismicity and reveal two major cluster across the foreshock and the mainshock, respectively.

## 3. Source process from broadband waveform analysis

### 3.1. Method and data

The waveform modeling method provides a rupture process of an earthquake as a sequence of double-couple point sources. These point sources are generally assumed to have the same fault plane. We employ a method developed by Kikuchi and Kanamori (1986, 1991), which allows for mechanism changes during the rupture sequence and is well suited to study earthquakes with complex rupture processes.

We analyze teleseismic P waves from 29 broadband seismograph stations with a good azimuthal coverage. The earthquake locations and origin times obtained in EHB processing (see Section 2 for details) are used as the initial parameters. To determine the P wave arrival times, we first use the ak135 travel-time table, and then adjust the onset times by a few seconds to account for the variations of travel times due to the lateral heterogeneities of the Earth. The start time of each record is set at 10 s before the ak135 arrival time with a total of 50 and 80 s

Table 2  
Structures used to compute Green's functions

$\alpha$ (km/s)	$\beta$ (km/s)	$\rho$ (g/cm <sup>3</sup> )	Thickness (km)
Source structure			
1.50	0.00	1.00	3.00
3.00	1.36	1.87	4.00
6.50	3.74	2.87	7.00
8.00	4.60	3.30	–
Receiver structure			
5.80	3.46	2.45	20.00
6.50	3.85	2.71	15.00
8.04	4.48	3.29	–

The near-source structure is from an OBS seismic experiment (Nakanishi et al., 2002) and the near-receiver structure is the ak135 model.

windows for the foreshock and the mainshock, respectively. Waveforms are band-pass-filtered from 0.01 to 2.0 Hz. Table 2 shows the velocity structures used to compute Green's functions. The near-source structure is

from an OBS seismic experiment (Nakanishi et al., 2002) and the near-receiver structure is the ak135 model.

### 3.2. The foreshock

The results of the teleseismic wave inversion of the foreshock are given in Table 3 and shown in Fig. 4. The waveform matches between the synthetic waves and the observed data are good at most stations. A high-angle reverse fault striking in nearly an east–west direction is predominant in the moment release. The total scalar seismic moment is about  $0.765 \times 10^{20}$  N m, which is equivalent to  $M_W$  7.2. The maximum dislocation,  $D_{\max} = 3.9$  m, appears close to the epicenter. The total duration of the source rupture process is about 15 s. The fault area is about  $50 \text{ km} \times 30 \text{ km}$ . Using the aftershock area,  $1200 \text{ km}^2$ , we obtain the average stress drop as  $\Delta\sigma = 2.5M_0/S^{1.5} = 4.2 \text{ MPa}$ , which is comparable

Table 3  
Source parameters of the foreshock and the mainshock for the final solution

Event	$\varphi_N$ (°)	$\lambda_E$ (°)	$H$ (km)	Str. (°)	Dip (°)	Slip (°)	Moment ( $\times 10^{20}$ N m)	$M_W$	$\Delta\sigma$ (MPa)
Foreshock	33.06	136.64	18.3	280	40	104	0.77	7.2	4.2
Mainshock	33.18	137.11	17.6				1.08	7.3	6.5
Primary				150	70	174			
Secondary				85	40	89			

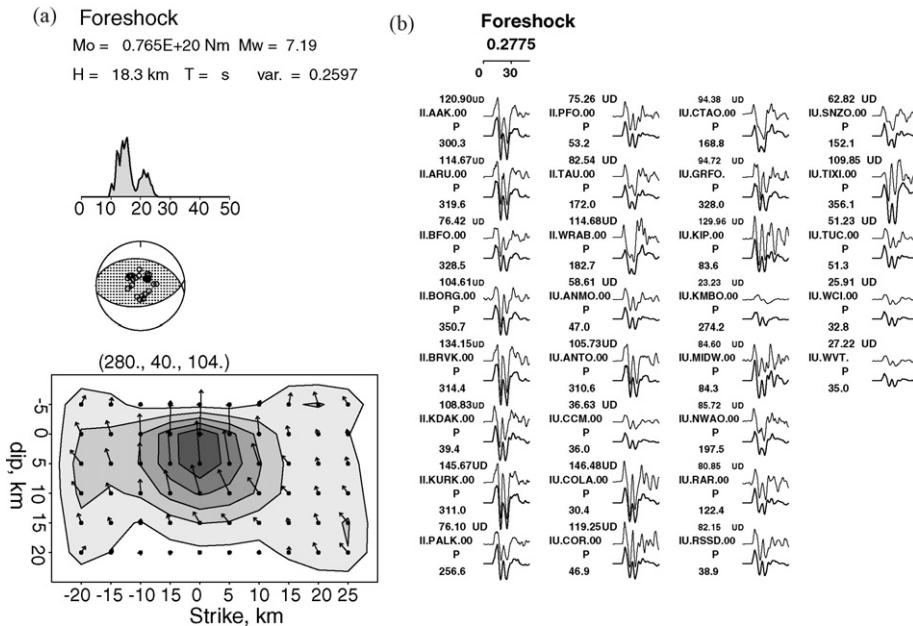


Fig. 4. (a) Obtained total moment rate function, mechanism, and distribution of coseismic slip. Coordinate (0,0) indicate the location of initial break. (b) Comparison of the observed records (upper trace) with synthetic waves (lower trace). They are displacement seismograms integrated from velocity records. The numbers on the upper and lower left indicate the peak-to-peak amplitude in micrometers of the observed record and the azimuth of the station to the earthquake, respectively. The synthetic waves are plotted with the same scale as the observed.

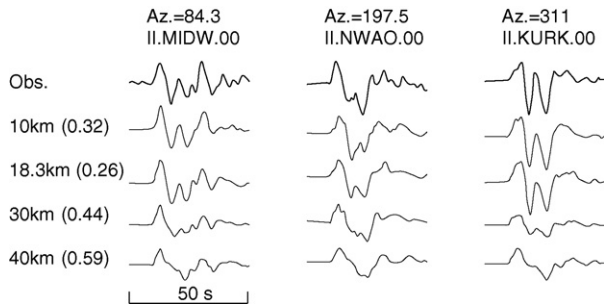


Fig. 5. Observed records (boldface traces) and synthetic waves (light-face traces) for four depths at three stations. They are displacement seismograms integrated from velocity records. The numbers above each figure indicate the azimuths of stations to the earthquake cluster. The numbers after the depth are variances between observed records and synthetic waves. The similarity between observed records and synthetic waves suggests that the best-fitting focal depth is 18.3 km.

to the typical value of 10 MPa for intraplate earthquakes (Kikuchi and Kanamori, 1991). We presume that the northward dipping fault plane is the primary fault plane according to the improved hypocenter distribution (Fig. 3(b)).

Fig. 5 shows synthetic waves for four depths and the observed data. The shape of the synthetic waves varies with focal depth due to the change of surface reflections in arrival times. The observed waveforms are similar to the synthetic waves for a depth of 18.3 km. This implies that the centroid depth obtained by waveform modeling is located close to the depth of the initial break obtained by the earthquake location.

### 3.3. The mainshock

We first obtain for the mainshock a southward dipping reverse fault striking in nearly an east–west direction. In this case, the overall agreement of the waveforms is good, but relatively large discrepancy is seen at the southeastern and northwestern stations. Such misfit in the particular azimuth suggests that some secondary subevents with a different source mechanism may exist. Also, aftershocks extended in both the northwest and the southwest directions from the location of the mainshock. It seems that the single fault plane is incomplete to explain the complex aftershock pattern. With these observations in mind, we consider a case where a source process consists of subevents with different fault planes.

The final results of the mainshock are given in Table 3 and shown in Fig. 6. This event consists of two subevents: a northwest-tending strike-slip event and a southward dipping thrust event. The total scalar seismic moment is about  $0.108 \times 10^{21}$  N m ( $M_W$  7.3). The maximum dislocation,  $D_{max} = 2.7$  m, appears in the shallow region updip of the hypocenter. The total duration of the source rupture process is about 20 s. The fault area is about 80 km  $\times$  50 km. The average stress drop is about 6.5 MPa, and the centroid depth is about 17.6 km.

### 4. Discussion and conclusions

The seismic activity started with the  $M_W$  7.2 foreshock (No. 1), on a northward dipping reverse fault striking in nearly an east–west direction. Between the

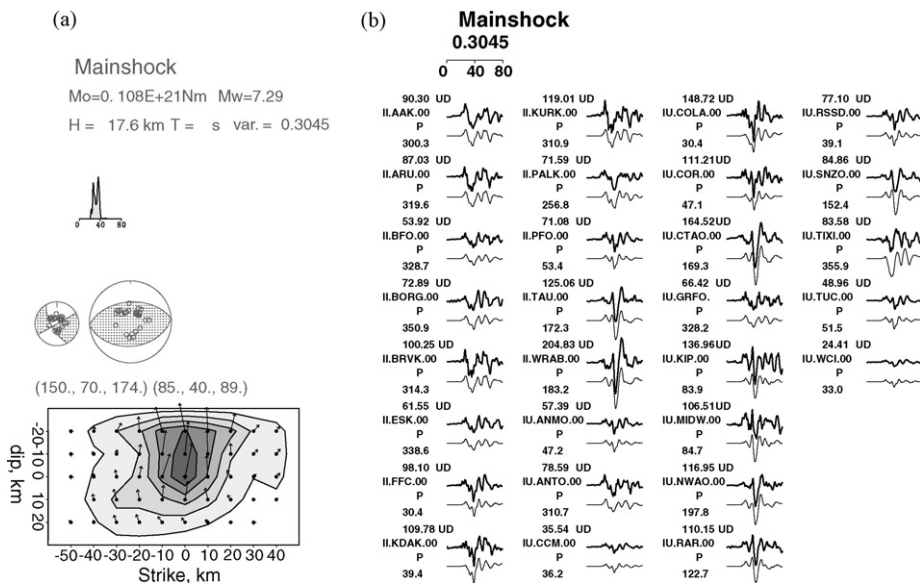


Fig. 6. The same as Fig. 4, but for the mainshock.

$M_W$  7.2 and the  $M_W$  7.3 events, many small events took place in the coseismic slip area of the  $M_W$  7.2 event. About 5 h after the  $M_W$  7.2 foreshock the  $M_W$  7.3 mainshock (No. 8) occurred with two different faults: a northwest-trending strike-slip fault and a southward dipping reverse fault striking in a nearly east–west direction. Aftershocks are located both to the northwest and the southwest from the mainshock. Two strong aftershocks (Nos. 32 and 37) occurred 2 and 3 days later, respectively, in a similar place with the mainshock. There were about 2500 aftershocks with magnitudes greater than 2.0 in a 1-year period. This feature is consistent with the idea that thrust earthquakes, unlike strike-slip ones, are more likely to be followed by strong aftershocks (Wu et al., 2004).

The events in this study were relocated in a depth range between 10 and 33 km, shallower by about 20 km than those by JMA. In a previous study (Bai et al., 2006), we relocated relatively smaller events using an improved double-difference earthquake location algorithm with regional sP depth phases. Several events are common to both studies and most of them have focal depth comparable with each other. The focal depths of earthquakes usually correlate with the effective elastic thickness ( $T_e$ ) (Maggi et al., 2000). The  $T_e$  of the PHS in the focal region, estimated from the seafloor age, is about 35 km (Yoshioka and Ito, 2001). Most JMA hypocenters that are deeper than 35 km might be over-estimated by the combination of poor azimuthal coverage and the use of an inappropriate travel time model. Earthquakes are mostly relocated in the uppermost mantle of the PHS, which are consistent with magnitude–depth correlations of intraplate seismicity in the PHS (Smith et al., 2004).

Focal mechanisms of smaller events were determined by Ito et al. (2005) and NIED (Japan National Research Institute for Earth Science and Disaster Prevention) using data from F-net (broad-band seismograph network). The dominant reverse fault set, including the four events with magnitudes greater than six, is almost parallel to the trough. Events with strike-slip mechanisms are mostly located to the northwest and the southeast from the mainshock. Previous studies (including the NIED and Harvard CMT) also revealed the main-shock with a high-angle reverse fault, which is different from the mega-thrust earthquake on a low-angle fault plane.

A total of nine large ( $M \geq 7$ ) compressional outer rise events is found by searching events listed in individual publications and the Harvard CMT catalog back to 1962. The outer rise events had almost the same compression axes with the following large mega-thrust events. The 2004 earthquakes with N–S compression axes, however, do not correspond to the plate-subduction direction of

NWW. This earthquake sequence is distributed at the westward prolongation of the Zenisu Ridge (Fig. 1(b)). Kinematic models predicted a 1 cm/year motion of the PHS relative to the Zenisu Ridge in nearly a N–S direction (Mazzotti et al., 1999), which seems to be consistent with the focal mechanisms. The 2004 earthquakes with N–S compression axes may suggest that the compressional stresses are accumulating in the Zenisu region.

## Acknowledgements

We are grateful to Prof. Hiroo Kanamori, and Prof. Yuzo Ishikawa for useful discussion. Constructive comments are due to Prof. George Hellfrich and two anonymous reviewers. The bathymetric data is taken from the Japan Oceanographic Data Center. The arrival times and waveforms are provided by the U.S. Geological Survey and IRIS Data Management Center. We used the General Mapping Tool (GMT) to make figures. This research was financially supported by a Sasakawa Scientific Research Grant from the Japan Science Society (17-064).

## References

- Bai, L., Kawasaki, I., Zhang, T.Z., Ishikawa, Y., 2006. An improved double-difference earthquake location algorithm using sP phases: application to the foreshock and aftershock sequences of the 2004 earthquake offshore of the Kii peninsula, Japan ( $M_W$  7.5). *Earth Planets Space* 58, 823–830.
- Bondár, I., Myers, S.C., Engdahl, E.R., Bergman, E.A., 2004. Epicentre accuracy based on seismic network criteria. *Geophys. J. Int.* 156, 483–496.
- Engdahl, E.R., 2006. Application of an improved algorithm to high precision relocation of ISC test events. *Phys. Earth Planet Int.* 158, 14–18.
- Engdahl, E.R., Hilst, R., Buland, R., 1998. Global teleseismic earthquake relocation with improved travel times and procedures for depth determination. *Bull. Seism. Soc. Am.* 88, 722–743.
- Engdahl, E.R., Jackson, J.A., Myers, S.C., Bergman, E.A., 2006. Relocation and assessment of seismicity in the Iran region. *Geophys. J. Int.* 167, 761–778.
- Ito, Y., Matsumoto, T., Kimura, H., Matsubayashi, H., Obara, K., Sekiguchi, S., 2005. Spatial distribution of centroid moment tensor solutions for the 2004 off Kii peninsula earthquakes. *Earth Planets Space* 57, 351–356.
- Jeffreys, H., Bullen, K.E., 1940. *Seismological Tables*. British Association for the Advancement of Science, London.
- Jordan, T.H., Sverdrup, K.A., 1981. Teleseismic location techniques and their application to earthquake clusters in the south-central Pacific. *Bull. Seism. Soc. Am.* 71, 1105–1130.
- Kanamori, H., 1972. Tectonic implications of the 1944 Tonankai and the 1946 Nankaido earthquakes. *Phys. Earth Planet Int.* 5, 129–139.
- Kennett, B.L.N., Engdahl, E.R., 1991. Travel times for global earthquake location and phase identification. *Geophys. J. Int.* 105, 429–465.

- Kennett, B.L.N., Engdahl, E.R., Buland, R., 1995. Constraints on seismic velocities in the Earth from traveltimes. *Geophys. J. Int.* 122, 403–416.
- Kikuchi, M., Kanamori, H., 1986. Inversion of complex body waves. II. *Phys. Earth Planet Int.* 43, 205–222.
- Kikuchi, M., Kanamori, H., 1991. Inversion of complex body waves. III. *Bull. Seism. Soc. Am.* 81, 2335–2350.
- Kikuchi, M., Nakamura, M., Yoshikawa, K., 2003. Source rupture process of the 1944 Tonankai earthquake and the 1945 Mikawa earthquake derived from low-gain seismograms. *Earth Planets Space* 55, 159–172.
- Maggi, A., Jackson, J.A., McKenzie, D., Priestley, K., 2000. Earthquake focal depths, effective elastic thickness, and the strength of the continental lithosphere. *Geology* 28, 495–508.
- Mazzotti, S., Henry, P., Pichon, X.L., Sagiya, T., 1999. Strain partitioning in the zone of transition from Nankai subduction to Izu-Bonin collision (Central Japan): implication for extensional tear within the subducting slab. *Earth Planet. Sci. Lett.* 172, 1–10.
- Nakanishi, A., Takahashi, N., Park, J.O., Miura, S., Kodaira, S., Kaneda, Y., Hirata, N., Iwasaki, T., Nakamura, M., 2002. Crustal structure across the coseismic rupture zone of the 1944 Tonankai earthquake, the central Nankai Trough seismogenic zone. *J. Geophys. Res.* 107, 2007, doi:10.1029/2001JB000424.
- Rastogi, B.K., Bergman, E.A., Engdahl, E.R., 2005. Improved earthquake locations and estimation of Pn and Sn path anomalies for India, using multiple event relocation and reference events. *Curr. Sci.* 88, 1586–1591.
- Richards, P.G., Waldhauser, F., Schaff, D., Kim, W.Y., 2006. The applicability of modern methods of earthquake location. *Pure Appl. Geophys.* 163, 351–372.
- Ritzwoller, M.H., Shapiro, N.M., Levshin, A.L., Bergman, E.A., Engdahl, E.R., 2003. Ability of a global three-dimensional model to locate regional events. *J. Geophys. Res.* 108, 2353, doi:10.1029/2002JB002167.
- Sakai, S., Yamada, T., Shinohara, M., Hagiwara, H., Kanazawa, T., Obana, K., Kodaira, S., Kaneda, Y., 2005. Urgent after-shock observation of the 2004 off the Kii peninsula earthquake using ocean bottom seismometers. *Earth Planets Space* 57, 363–368.
- Seno, T., Stein, S., Gripp, A.E., 1993. A model for the motion of the Philippine Sea plate consistent with NUVEL-1 and geological data. *J. Geophys. Res.* 98, 17941–17948.
- Smith, A.J., Cummins, P.R., Baba, T., Kodaira, S., Kaneda, Y., Yamaguchi, H., 2004. Intra-plate seismicity in the subducting Philippine Sea Plate, southwest Japan: magnitude-depth correlations. *Phys. Earth Planet Int.* 145, 179–202.
- The Headquarter of Earthquake Research Promotion, 2001. On the Long-term Evaluation of Earthquakes in the Nankai Trough. <http://www.jishin.go.jp> (in Japanese).
- Wu, Z.L., Wan, Y.G., Zhou, G.W., 2004. Focal mechanism dependence of a few seismic phenomena and its implications for the physics of earthquakes. *Pure Appl. Geophys.* 161, 1969–1978.
- Wu, S.G., Takahashi, N., Tokuyama, H., Wong, H.K., 2005. Geomorphology, sedimentary processes and development of the Zenisu deep-sea channel, northern Philippine Sea. *Geo-Marine Letters* 25, 230–240.
- Yoshioka, S., Ito, Y., 2001. Lateral variations of effective elastic thickness of the subducting Philippine Sea plate along the Nankai trough. *Earth Planets Space* 53, 261–273.